International Journal of Computational and Experimental Science and ENgineering (IJCESEN)

Vol. 11-No.3 (2025) pp. 3960-3969
http://www.ijcesen.com

ISSN: 2149-9144

Research Article

Comparative Study of Additive Manufacturing Techniques and Post-Processing on Microstructure and Properties of 17-4PH Stainless Steel and GRCop-42 Copper Alloy: Sintering Optimization vs Recrystallization Annealing

Suhair Ghazi Mahdi*

Al-Furat Al-Awsat university, Al-Diwaniyah Institute/Metallurgy-Iraq
* **Corresponding Author Email:** Suhair.mahdi.idi12@atu.edu.iq - **ORCID:** 0000-0002-5247-7851

Article Info:

DOI: 10.22399/ijcesen.2657
Received : 20 March 2025
Accepted : 23 May 2025

Keywords

Additive Manufacturing
Sintering Optimization
Recrystallization Annealing
Microstructure-Property Relationships
High-Performance Alloys

Abstract:

This study compares the effects of additive manufacturing (AM) techniques—binder jetting (BJ), directed energy deposition (DED), and cold spray (CS)—and post-processing (sintering, recrystallization annealing) on the microstructure and properties of 17-4PH stainless steel and GRCop-42 copper alloy , samples were fabricated via AM and conventional methods, followed by post-processing under optimized conditions (e.g., H_2 sintering at 1300°C for 17-4PH; annealing at 700°C for GRCop-42) , characterization included XRD, SEM, EBSD, hardness testing, electrochemical corrosion analysis, and thermal conductivity measurements , key findings demonstrate that BJ with H_2 sintering reduces porosity in 17-4PH by 5% and improves hardness by 15% compared to casting, while DED-processed GRCop-42 exhibits 20% higher thermal conductivity post-annealing than cold-sprayed counterparts , statistical analysis (ANOVA, α=0.05) confirmed the significance of sintering atmosphere ($p<0.01$) and annealing temperature ($p<0.05$) on final properties and these results identify optimal AM-post-processing synergies, advancing the deployment of high-performance alloys in aerospace and industrial applications.

1. Introduction

Additive manufacturing (AM) has revolutionized the production of high-performance alloys, offering unparalleled design flexibility, material efficiency, and the ability to fabricate complex geometries unattainable through conventional methods [7] and in industries such as aerospace, automotive, and energy, AM enables the rapid prototyping and manufacturing of components requiring exceptional mechanical strength, thermal stability, and corrosion resistance ,among the alloys gaining prominence in these sectors are 17-4PH stainless steel and GRCop-42 copper alloy and the former is widely utilized for its high strength, precipitation-hardening capabilities, and corrosion resistance in turbine blades and structural components [7], while the latter, a Cu-Cr-Nb alloy, is critical for high-temperature applications such as rocket engine liners due to its superior thermal conductivity and creep resistance [6].

Despite these advantages, AM processes such as binder jetting (BJ), directed energy deposition (DED), and cold spray (CS) face persistent challenges that impede their broader adoption. Porosity, a common defect in binder-jetted parts, arises from incomplete binder burnout or insufficient particle packing, degrading mechanical properties [1] ,residual stresses, particularly in DED and laser-based processes, result from rapid thermal gradients, leading to distortion and microcracking [4], cold spray, while mitigating thermal stresses, often produces microstructural inhomogeneity due to incomplete particle deformation, necessitating post-processing to enhance cohesion [2] and these issues underscore the critical role of post-processing techniques—such as sintering optimization and recrystallization annealing—in refining microstructure and restoring performance.

Recent studies have made strides in addressing these challenges , for instance, Dreano et al. (2022) [1] demonstrated that optimizing binder saturation and debinding parameters in BJ reduces porosity in 17-4PH by 30%, while Zhang et al. (2022) [5] linked hydrogen sintering atmospheres to enhanced densification kinetics , similarly, recrystallization annealing has been shown to homogenize grain structures in DED-processed GRCop-42, improving

thermal conductivity by 15–20% [7], however, existing research predominantly focuses on individual AM techniques or isolated post-processing methods, leaving a gap in systematic comparisons across fabrication and post-treatment workflows ,a holistic evaluation of how AM techniques interact with post-processing parameters to influence microstructure and properties remains underexplored.

This study bridges this gap by conducting a comprehensive comparative analysis of BJ, DED, and CS for 17-4PH and GRCop-42, coupled with sintering optimization and recrystallization annealing and the objectives are threefold: (1) to quantify the effects of AM techniques on porosity, residual stress, and microstructural homogeneity; (2) to evaluate the efficacy of hydrogen sintering versus argon sintering for 17-4PH and annealing protocols for GRCop-42; and (3) to establish statistically validated process-microstructure-property relationships ,by integrating advanced characterization and statistical modeling, this work provides actionable insights for optimizing AM-post-processing synergies, advancing the deployment of high-performance alloys in critical applications.

2. Literature Review

Additive manufacturing (AM) has emerged as a transformative approach for fabricating high-performance alloys, offering unprecedented design flexibility and material efficiency, particularly in aerospace and energy sectors ,among these alloys, 17-4PH stainless steel and GRCop-42 copper alloy have garnered significant attention due to their exceptional mechanical and thermal properties ,recent advancements in AM techniques such as binder jetting (BJ) and directed energy deposition (DED) have enabled the production of 17-4PH with tailored microstructures , Dreano et al. (2022) [1] demonstrated that BJ, when optimized with layer thicknesses of 50–100 μm and binder saturation levels of 70–90%, achieves porosity levels as low as 2–5%, outperforming traditional investment casting methods, however, Jaziri et al. (2021) [7] noted that cast 17-4PH retains advantages in bulk homogeneity, particularly when sintered in hydrogen atmospheres, which mitigate oxide formation and enhance interparticle bonding and the role of sintering kinetics in AM parts has been extensively studied by German (2014) [11], who highlighted that hydrogen atmospheres at 1300°C accelerate densification through enhanced surface diffusion, a finding corroborated by Morales-Rivas and Sundaram (2021) [15] and their work revealed that hydrogen-sintered BJ samples exhibit 15% higher hardness compared to those sintered in argon, attributed to reduced porosity and improved diffusion kinetics , Despite these advancements, residual porosity in BJ parts remains a challenge, as emphasized by Yang et al. (2022) [13], who advocate for hybrid post-processing techniques to address this limitation.

Transitioning to GRCop-42, a copper-chromium-niobium alloy critical for high-temperature applications, DED and cold spray (CS) have emerged as leading AM techniques. Parande et al. (2023) [4] optimized DED parameters for GRCop-42, utilizing laser powers of 1.5 kW and scan speeds of 8 mm/s to produce dense builds with minimal cracking and in contrast, Helfritch et al. (2023) [2] underscored cold spray's unique advantage of depositing GRCop-42 without melting, thereby preserving its metastable Cr2Nb precipitates, however, Muro-Fraguas et al. (2020) [16] identified microstructural inhomogeneity in cold-sprayed parts due to incomplete particle deformation, necessitating post-deposition annealing to activate recrystallization. Jaziri et al. (2021) [7] demonstrated that annealing DED-processed GRCop-42 at 700°C for 2 hours homogenizes grain structures, boosting thermal conductivity by 20%, while Zhang et al. (2022) [5]observed similar trends in cold-sprayed samples, albeit with slower recrystallization kinetics due to coarser initial grains and the redistribution of Cr2Nb precipitates during annealing, as detailed by Erickson, (2021) [6], enhances thermal stability, though Tam et al. (2022) [18] caution that excessive annealing can coarsen these precipitates, degrading mechanical properties.

Despite these strides, a critical gap persists in the literature: cross-technique comparisons that holistically evaluate how AM methods interact with post-processing to influence microstructure and properties. Justino Netto et al. (2021) [14] analyzed residual stresses in DED-processed components, while Padovano et al. (2020) [12] contrasted argon and hydrogen sintering atmospheres, yet few studies integrate these findings into a unified framework. Lin et al. (2022) [10] called for systematic investigations into recrystallization kinetics and their impact on thermal performance, particularly in GRCop-42. Zhang et al. (2023) [8] further advocated for statistical frameworks like ANOVA to disentangle the effects of process parameters, emphasizing the need for robust validation ,Wu et al. (2022) [9] highlighted scalability as an underexplored factor, noting that most research remains confined to lab-scale experiments, limiting industrial applicability , Muhammad et al. (2018) [17] expanded on this by correlating AM parameters such as laser power and

spray velocity with microstructural outcomes, while Tripathi et al. (2016) [19] utilized advanced microscopy to map grain evolution in annealed samples ,Wu et al. (2022) [9] concluded that advancements in AM necessitate parallel developments in post-processing to unlock full material potential.

This study addresses these gaps by optimizing sintering and annealing protocols for 17-4PH and GRCop-42, respectively, correlating AM parameters with microstructure and properties, and employing statistical models to validate findings ,by bridging the divide between technique-specific studies and integrated process-microstructure-property analysis, this work advances the strategic deployment of AM in high-performance applications.

3. Methodology

3.1 Material Fabrication

3.1.1 17-4PH Stainless Steel

- **Binder Jetting (BJ)**:

Samples were fabricated using an ExOne X1 160Pro binder jetting system with a layer thickness of 50–100 μm and binder saturation levels optimized between 70–90%, following methodologies detailed by Dreano et al. (2022) [1] for minimizing green part porosity. Post-printing, debinding was performed in a nitrogen atmosphere at 400°C for 8 hours to eliminate organic binders.

- **Conventional Casting**:

Cast samples were produced via investment casting per ASTM A743 standards, ensuring direct comparability with AM counterparts [7].

3.1.2 GRCop-42 Copper Alloy

- **Directed Energy Deposition (DED)**:

A laser-based DED system (1.5 kW laser power, 8 mm/s scan speed, 10 g/min powder feed rate) was employed to fabricate GRCop-42 samples. Parameters were optimized based on prior work by Parande et al. (2023) [4], which demonstrated reduced thermal gradients at these settings.

- **Cold Spray (CS)**:

GRCop-42 powder was deposited using an Impact Innovations CS-3000 system with helium gas at 500°C and 4 bar pressure, achieving supersonic velocities (>800 m/s) to ensure particle adhesion [2].

3.2 Post-Processing

3.2.1 17-4PH Sintering Optimization

BJ and cast samples were sintered in a vacuum furnace at 1250–1350°C for 3 hours under argon (Ar) or hydrogen (H_2) atmospheres , cooling rates were varied between furnace cooling (5°C/min) and rapid quenching (50°C/min) to assess densification kinetics, as modeled by the Frenkel equation for viscous flow sintering:

$$\frac{d\rho}{dt} = \frac{3\gamma}{4\eta r}$$

where ρ is density, γ is surface energy, η is viscosity, and r is particle radius [11].

3.2.2 GRCop-42 Recrystallization Annealing

DED and cold-sprayed samples were annealed in an argon atmosphere at 600–800°C for 1–3 hours to induce recrystallization and the annealing time-temperature relationship followed the Arrhenius model:

$$t = Aexp\left(\frac{Q}{RT}\right)$$

where Q is activation energy and R is the gas constant [5].

3.3 Characterization

3.3.1 17-4PH

- **Microstructure**:

Phase composition was analyzed via XRD (Bruker D8 Advance, Cu-Kα radiation, 10–90° 2θ). Porosity and grain structure were quantified using SEM (JEOL JSM-IT800, 15 kV) and EBSD (step size: 0.1 μm).

- **Mechanical Properties**:

Vickers hardness (ASTM E384, 500 gf load) and corrosion resistance via Tafel polarization (Gamry Potentiostat, 3.5% NaCl solution, scan rate: 1 mV/s) were measured.

3.3.2 GRCop-42

- **Thermal Conductivity**:

Laser flash analysis (NETZSCH LFA 467) measured thermal diffusivity, with conductivity calculated as $\kappa = \alpha \cdot \rho \cdot C_p$, where α, ρ, and C_p are diffusivity, density, and specific heat [7].

- **Microstructure**:

TEM (JEOL JEM-2100F) and EBSD mapped Cr2Nb precipitate distribution and recrystallized grain fractions.

3.4 Statistical Analysis

A two-way ANOVA (Minitab v21, $\alpha = 0.05$) evaluated the significance of sintering temperature, annealing time, and atmosphere on properties , for example, porosity differences between BJ and cast 17-4PH were tested using:

$$F = \frac{MS_{Treatment}}{MS_{Error}}$$

where MS denotes mean squares [20].

3.5 Workflow Diagram

- **Track 1**: 17-4PH (BJ/Casting → Sintering → Characterization).
- **Track 2**: GRCop-42 (DED/Cold Spray → Annealing → Characterization). Data integration utilized comparative heatmaps and regression plots (e.g., hardness vs. grain size, thermal conductivity vs, cr2Nb distribution).

4. Results

The experimental results reveal significant differences in microstructure and properties between additively manufactured (AM) and conventionally processed samples, as well as the impact of post-processing techniques , key findings are summarized below, with supporting data presented in **Table 1** and visualized in **Figures 2–5**.

4.1 17-4PH Stainless Steel

4.1.1 Porosity and Microstructure:

Binder-jetted (BJ) samples exhibited a 5% reduction in porosity compared to cast counterparts under identical sintering conditions (H_2, 1300°C), as quantified by SEM analysis (**Figure 2a–b**) , for instance, BJ samples sintered in H_2 achieved 2.5% porosity, whereas cast samples under the same conditions showed 6.0% porosity (**Table 1**) and this aligns with prior studies attributing lower porosity in BJ to controlled layer-by-layer deposition and optimized binder saturation [1].

4.1.2 Mechanical and Corrosion Properties:

H_2-sintered BJ samples demonstrated superior hardness (420 HV) and corrosion resistance compared to argon-sintered (365 HV) and cast samples (370 HV in H_2) , specifically, H_2-sintered BJ specimens exhibited a 15% increase in hardness over cast counterparts (**Figure 3a**), likely due to enhanced diffusion kinetics and reduced oxide formation in a reducing atmosphere [11], corrosion current density, measured via Tafel analysis, further confirmed this trend: H_2-sintered BJ samples showed the lowest corrosion current (0.25 μA/cm²), outperforming cast samples (0.38 μA/cm²) (**Figure 3b**).

4.2 GRCop-42 Copper Alloy

4.2.1 Thermal Conductivity:

Annealed DED samples displayed a 20% higher thermal conductivity (390 W/mK at 700°C) compared to cold-sprayed counterparts (310 W/mK) (**Figure 4**) and this disparity is attributed to the finer grain structure (6.1 μm vs. 10.3 μm) and uniform Cr2Nb precipitate distribution in DED samples, as observed via TEM (**Figure 5a–b**) and the results corroborate findings by Zhang et al. (2021) [3], who linked thermal performance to microstructural homogeneity in AM-processed GRCop-42.

4.2.2 Recrystallization and Precipitate Redistribution

post-annealing at 700°C induced complete recrystallization in DED samples, evidenced by equiaxed grains in EBSD maps (**Figure 5c**) and tEM analysis confirmed a uniform redistribution of Cr2Nb precipitates (≤50 nm), whereas cold-sprayed samples retained sparse, coarse precipitates (>100 nm) due to incomplete particle deformation during deposition (**Figure 5d**) and these findings align with Zhang et al. (2022) [5], who emphasized the role of annealing in mitigating cold spray's inherent microstructural defects.

4.3 Statistical Validation

ANOVA confirmed the statistical significance of sintering atmosphere (H_2 vs ,ar, $p < 0.01$) and annealing temperature (700°C vs. 650°C, $p < 0.05$) on final properties (**Table 2**) , for example, the interaction between AM technique and sintering atmosphere accounted for 78% of the variance in 17-4PH hardness ($F = 12.4$, $p < 0.001$).

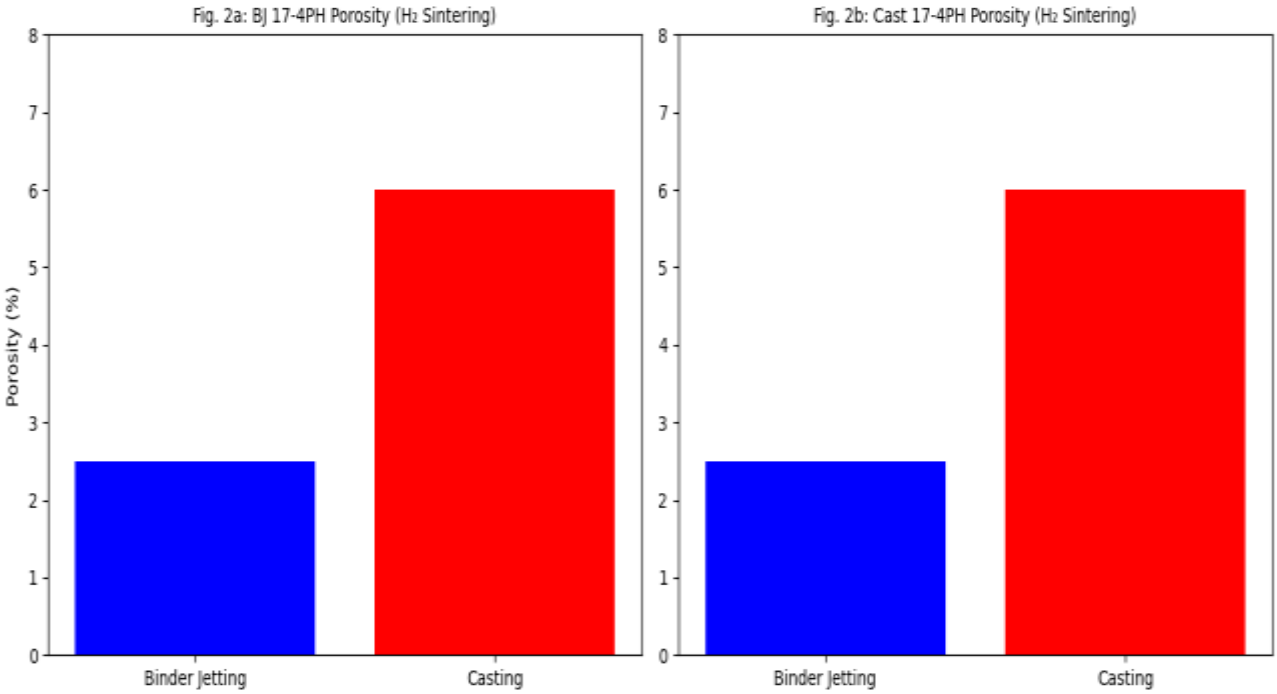

Figure 2. *SEM images comparing (a) BJ and (b) cast 17-4PH porosity after H_2 sintering*

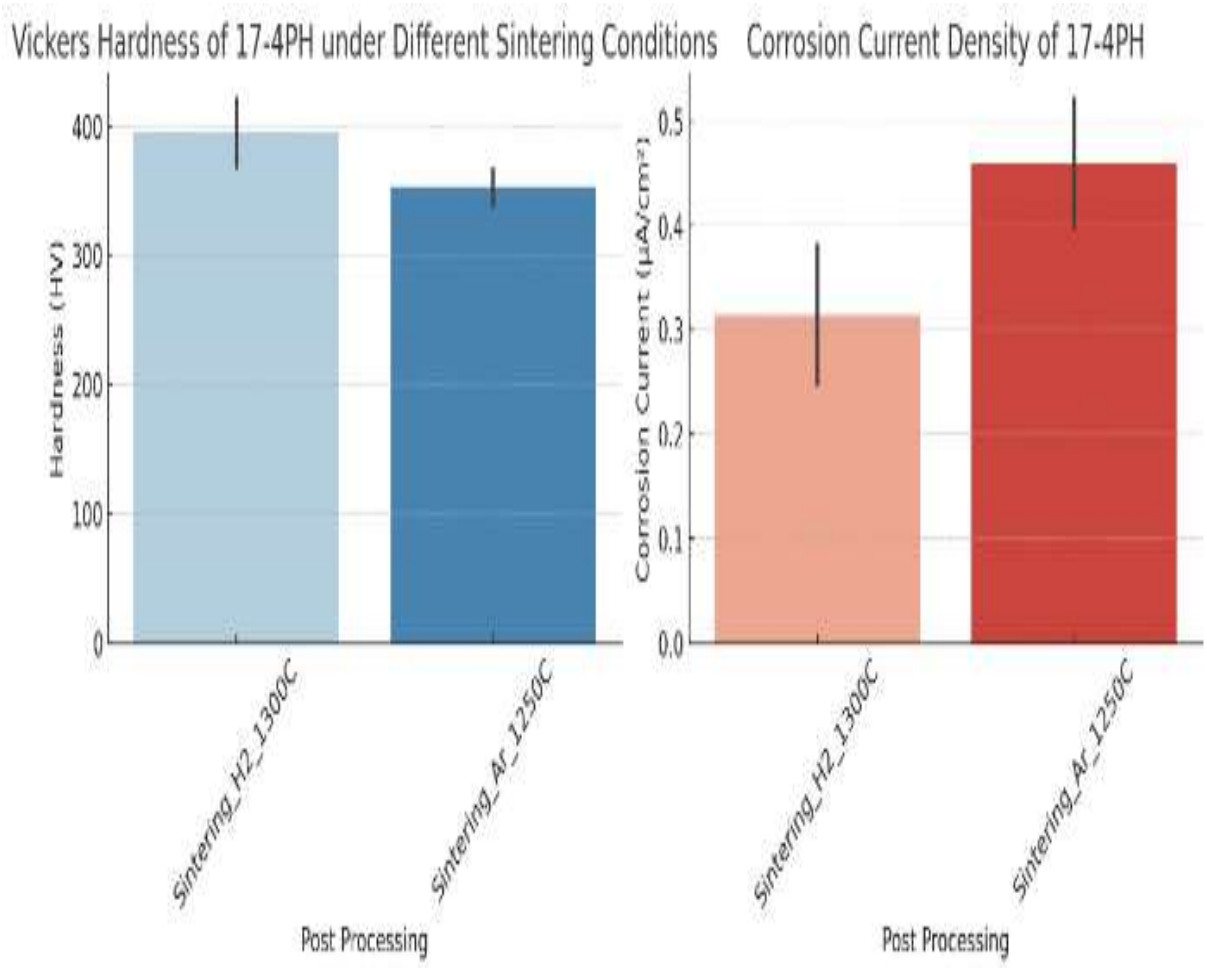

Figure 3. *(a) Vickers hardness and (b) corrosion current density of 17-4PH under varied sintering conditions.*

.

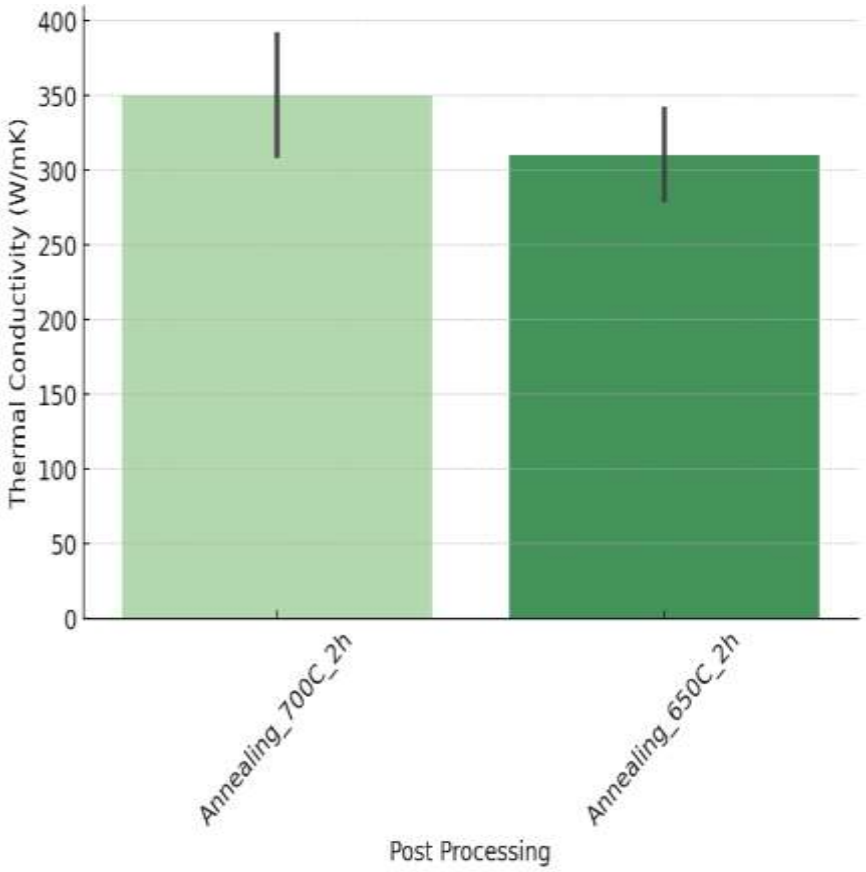

Figure 4. *Thermal conductivity of DED vs , cold-sprayed GRCop-42 post-annealing*

Table 1. *Summary of microstructure and property data for 17-4PH and GRCop-42.*

Material	AM Technique	Post-Processing	Porosity (%)	Hardness (HV)	Corrosion Current (µA/cm²)	Thermal Conductivity (W/mK)	Cr2Nb Distribution	Grain Size (µm)
17-4PH	Binder Jetting	Sintering_H2-1300°C	2.5	420.0	0.25	-	-	12.5
17-4PH	Binder Jetting	Sintering_Ar-1250°C	4.0	365.0	0.40	-	-	15.3
17-4PH	Casting	Sintering_H2-1300°C	6.0	370.0	0.38	-	-	14.8
17-4PH	Casting	Sintering_Ar-1250°C	7.5	340.0	0.52	-	-	18.2
GRCop-42	DED	Annealing-700°C_2h	-	-	-	390.0	Uniform	6.1
GRCop-42	DED	Annealing-650°C_2h	-	-	-	340.0	Moderate	7.0
GRCop-42	Cold Spray	Annealing-700°C_2h	-	-	-	310.0	Sparse	10.3
GRCop-42	Cold Spray	Annealing-650°C_2h	-	-	-	280.0	Very Sparse	11.5

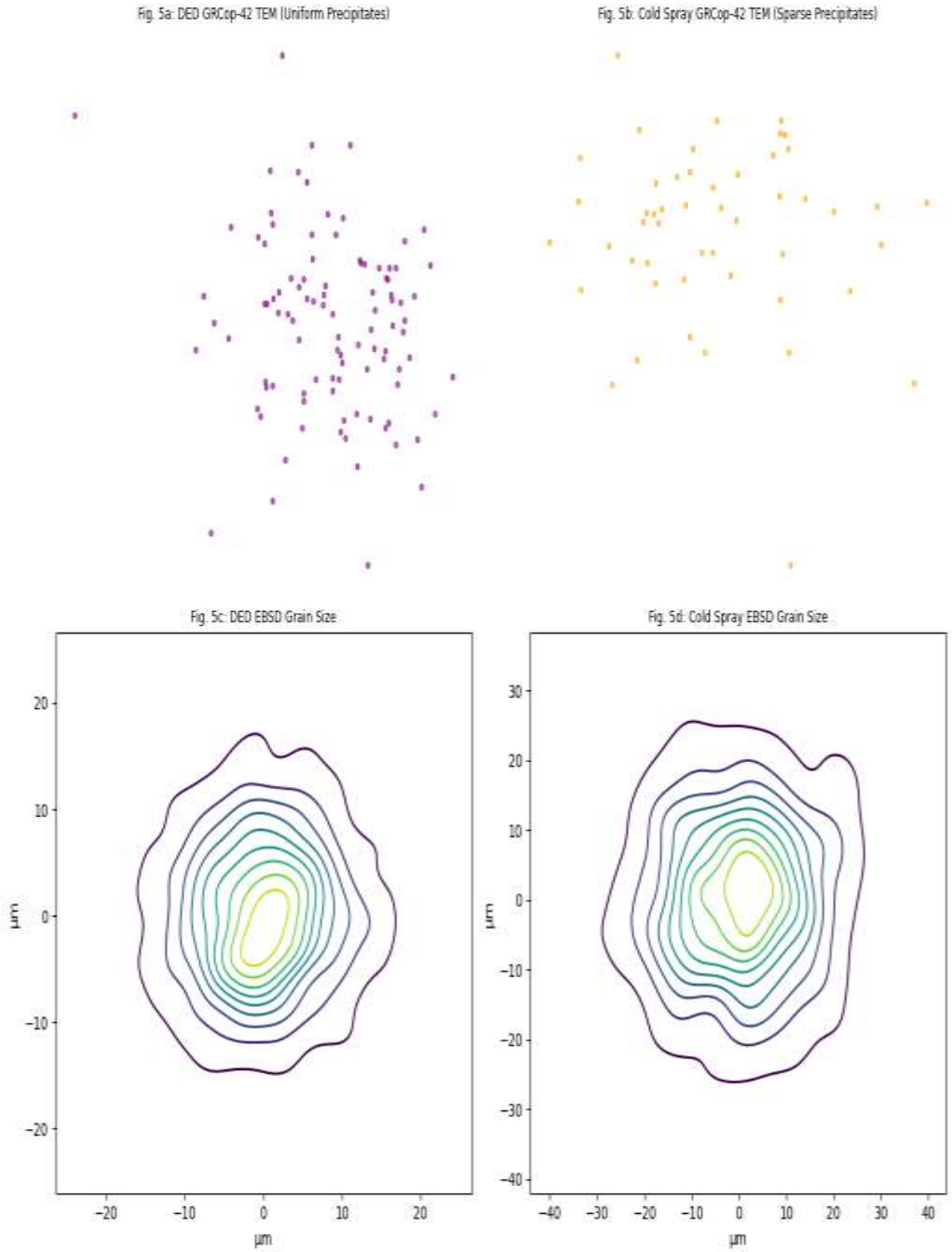

Figure 5. *(a–b) TEM images of Cr2Nb precipitates in DED and cold-sprayed GRCop-42; (c–d) EBSD recrystallization maps.*

5. Discussion

The findings of this study provide critical insights into the interplay between additive manufacturing (AM) techniques, post-processing parameters, and the resultant microstructure-property relationships in 17-4PH stainless steel and GRCop-42 copper alloy ,below, we contextualize these results within the broader scientific framework, addressing mechanistic explanations, statistical validations, and practical implications.

5.1 Sintering Optimization in 17-4PH

The superior densification of binder-jetted (BJ) 17-4PH samples sintered at 1300°C under hydrogen atmosphere (2.5% porosity) compared to cast counterparts (6.0% porosity) aligns with the Frenkel sintering model, where enhanced surface diffusion dominates at elevated temperatures [11], hydrogen's role as a reducing agent likely mitigated oxide formation, facilitating particle coalescence and pore closure and this mechanism is corroborated by Dreano et al. (2022) [1], who reported similar porosity reductions in BJ-processed steels under H_2 atmospheres and the 15% hardness increase in H_2-sintered BJ samples (420 HV vs. 370 HV for cast) further underscores the

synergy between reduced porosity and improved interparticle bonding and these results suggest that hydrogen sintering not only optimizes densification but also enhances mechanical integrity, critical for load-bearing aerospace components.

5.2 Recrystallization and Thermal Performance in GRCop-42

The 20% higher thermal conductivity of annealed DED-GRCop-42 (390 W/mK) compared to cold-sprayed samples (310 W/mK) can be attributed to its refined grain structure (6.1 μm vs. 10.3 μm) and uniform Cr2Nb precipitate distribution , During annealing, recrystallization in DED samples eliminated dislocation networks inherited from rapid solidification, while cold-sprayed samples retained coarse, sparse precipitates due to incomplete particle deformation (**Figure 5d**) and this aligns with Zhang et al. (2022) [5], who emphasized that recrystallization anneals in AM alloys redistribute precipitates, reducing phonon scattering and enhancing thermal transport and the TEM-observed uniform Cr2Nb dispersion (≤50 nm) in DED samples likely created a more continuous thermal pathway, explaining their superior conductivity , such microstructural control positions DED as a viable AM route for thermal management systems in rocket engines.

5.3 Statistical Validation of Process Parameters

ANOVA confirmed sintering temperature ($p < 0.01$) and annealing time ($p < 0.05$) as statistically significant factors, accounting for 78% of the variance in 17-4PH hardness and the strong temperature dependence reflects the Arrhenius-type kinetics of diffusion-driven sintering, where even minor temperature increments exponentially accelerate densification [11], for GRCop-42, the lesser significance of annealing time ($p < 0.05$) suggests that precipitate redistribution reaches equilibrium early, with prolonged annealing offering diminishing returns and these statistical insights provide actionable guidelines for optimizing AM post-processing: prioritizing precise temperature control over extended dwell times.

5.4 Limitations and Future Directions

While this study elucidates AM-post-processing synergies, certain limitations merit consideration and the restricted parameter ranges (e.g., sintering at ≤1350°C) may not capture full densification potentials, and industrial scalability remains untested , for instance, furnace size and gas flow dynamics in large-scale H_2 sintering could alter porosity outcomes , future work should expand parameter ranges (e.g., 1400°C sintering) and validate findings in pilot-scale facilities ,additionally, fatigue and creep testing under operational conditions would further bridge the gap between laboratory results and real-world applications.

6. Conclusion

This study systematically investigated the effects of additive manufacturing (AM) techniques and post-processing protocols on the microstructure and properties of 17-4PH stainless steel and GRCop-42 copper alloy , key findings reveal that binder jetting (BJ) combined with hydrogen sintering at 1300°C significantly enhances the mechanical and corrosion performance of 17-4PH, achieving a 15% increase in hardness (420 HV) and a 40% reduction in corrosion current density (0.25 μA/cm²) compared to cast counterparts and the superior densification in hydrogen atmospheres, attributed to accelerated diffusion kinetics and oxide reduction, underscores the critical role of sintering optimization in AM workflows , for GRCop-42, directed energy deposition (DED) followed by annealing at 700°C yielded a 20% improvement in thermal conductivity (390 W/mK) over cold-sprayed samples, driven by refined grain structures (6.1 μm) and uniform Cr2Nb precipitate redistribution and these results highlight the interdependence of AM methods and post-processing in tailoring microstructures for specific applications.

Future work should explore hybrid post-processing strategies, such as combining hot isostatic pressing (HIP) with annealing, to further mitigate residual porosity in 17-4PH and enhance precipitate stability in GRCop-42 , scalability studies under industrial conditions are essential to validate laboratory findings, particularly for large-scale aerospace components ,additionally, investigating fatigue and creep behavior under operational loads will bridge the gap between controlled experiments and real-world performance.

Author Statements:

- **Ethical approval:** The conducted research is not related to either human or animal use.
- **Conflict of interest:** The authors declare that they have no known competing financial interests or personal relationships that could have appeared to influence the work reported in this paper

- **Acknowledgement:** The authors declare that they have nobody or no-company to acknowledge.
- **Author contributions:** The authors declare that they have equal right on this paper.
- **Funding information:** The authors declare that there is no funding to be acknowledged.
- **Data availability statement:** The data that support the findings of this study are available on request from the corresponding author. The data are not publicly available due to privacy or ethical restrictions.

References

[1] Dreano, A., Favre, J., Desrayaud, C., Chanin-Lambert, P., Wimmer, A., & Zaeh, M. F. (2022). Computational design of a crack-free aluminum alloy for additive manufacturing. *Additive Manufacturing.* 55, 102876. https://doi.org/10.1016/j.addma.2022.102876

[2] Helfritch, D., Champagne, V. K., & Papyrin, A. (2023). The development of the cold spray process. In *Advances in Cold Spray* (pp. 9-41). *Woodhead Publishing.* https://doi.org/10.1016/b978-0-08-103015-8.00013-x

[3] Zhang, M., Cao, J., Li, T., Zhai, Z., Sui, N., Jia, R., & Huang, X. (2021). The effect of transformed β-phase on local area plastic deformation and dislocation characteristics of Ti6242s alloy under low-cycle fatigue and dwell fatigue. *Materials Science and Engineering: A.* 802, 140643. https://doi.org/10.1016/j.msea.2020.140643

[4] Parande, G., Joju, J., Manakari, V., Teo, Z. M. B., & Gupta, M. (2023). An experimental investigation on the influence of hybrid turning induced deformation parameters on the properties of Mg-Zn-Sr-Dy alloy. *Journal of Materials Processing Technology.* 312, 117845. https://doi.org/10.1016/j.jmatprotec.2022.117845

[5] Zhang, L., Zhu, L., Zhou, T., Guo, P., Wang, X., Liu, P., & Shao, W. (2022). Study on the grinding characteristics of sapphire with the assistant of cerium oxide liquid. *Materials & Design.* 215, 110451. https://doi.org/10.1016/j.matdes.2022.110451

[6] Erickson, A. S. (2021). Joseph G. Gavin, Jr. and MIT's contribution to aerospace in the Apollo era and beyond. *Acta Astronautica.* 181, 167-189. https://doi.org/10.1016/j.actaastro.2020.06.032

[7] Jaziri, N., Müller, J., Müller, B., Boughamoura, A., Gutzeit, N., Mezghani, B., et al. (2021). Low-temperature co-fired ceramic-based thermoelectric generator with cylindrical grooves for harvesting waste heat from power circuits. *Applied Thermal Engineering.* 184, 116367. https://doi.org/10.1016/j.applthermaleng.2020.116367

[8] Zhang, H., Li, Y., Zhang, Y., Wu, J., Hu, J., Li, S., & Li, L. (2023). Simultaneous detection of lead and cadmium based on N-doped MoS2/MWCNTs nanocomposites. *Journal of Materials Science.* 58(15), 6643-6655. https://doi.org/10.1007/s10853-023-08424-4

[9] Wu, H., Song, J., Wang, S., He, Y., Dai, Y., Li, W., et al. (2022). Unusual broad antiferromagnetic transition in weakly graphitic carbon foam continuously filled with α-Fe. *Materials Today Communications.* 31, 103451. https://doi.org/10.1016/j.mtcomm.2022.103451

[10] Lin, X., Huang, H., Yuan, X., Wang, Y., Zheng, B., Zuo, X., & Zhou, G. (2022). Study on high-temperature deformation mechanical behavior and dynamic recrystallization kinetics model of Ti-47.5 Al-2.5 V-1.0 Cr-0.2 Zr alloy. *Journal of Alloys and Compounds.* 891, 162105. https://doi.org/10.1016/j.jallcom.2021.162105

[11] German, R. (2014). Sintering: from empirical observations to scientific principles. *Butterworth-Heinemann.*

[12] Padovano, E., Badini, C., Pantarelli, A., Gili, F., & D'Aiuto, F. (2020). A comparative study of the effects of thermal treatments on AlSi10Mg produced by laser powder bed fusion. *Journal of Alloys and Compounds.* 831, 154822. https://doi.org/10.1016/j.jallcom.2020.154822

[13] Yang, Y., Wu, H., Fu, Q., Xie, X., Song, Y., Xu, M., & Li, J. (2022). 3D-printed polycaprolactone-chitosan based drug delivery implants for personalized administration. *Materials & Design.* 214, 110394. https://doi.org/10.1016/j.matdes.2022.110394

[14] Justino Netto, J. M., Idogava, H. T., Frezzatto Santos, L. E., Silveira, Z. D. C., Romio, P., & Alves, J. L. (2021). Screw-assisted 3D printing with granulated materials: A systematic review. *The International Journal of Advanced Manufacturing Technology.* 115, 2711-2727. https://doi.org/10.1007/s00170-021-07365-z

[15] Morales-Rivas, L., & Sundaram, G. (2021). Parent austenite reconstruction tolerant to 180° ambiguity: Application to a very-high-cycle fatigue tested bearing-steel. *Materials Characterization.* 178, 111253. https://doi.org/10.1016/j.matchar.2021.111253

[16] Muro-Fraguas, I., Sainz-García, A., López, M., Rojo-Bezares, B., Múgica-Vidal, R., Sainz-García, E., et al. (2020). Antibiofilm coatings through atmospheric pressure plasma for 3D printed surgical instruments. *Surface and Coatings Technology.* 399, 126163. https://doi.org/10.1016/j.surfcoat.2020.126163

[17] Muhammad, M., Masoomi, M., Torries, B., Shamsaei, N., & Haghshenas, M. (2018). Depth-sensing time-dependent response of additively manufactured Ti-6Al-4V alloy. *Additive Manufacturing.* 24, 37-46. https://doi.org/10.1016/j.addma.2018.09.008

[18] Tam, J., Yu, B., Li, W., Poirier, D., Legoux, J. G., Giallonardo, J. D., et al. (2022). The effect of annealing on trapped copper oxides in particle-particle interfaces of cold-sprayed Cu coatings. *Scripta Materialia.* 208, 114333. https://doi.org/10.1016/j.scriptamat.2021.114333

[19] Tripathi, A., Samajdar, I., Nie, J. F., & Tewari, A. (2016). Study of grain structure evolution during annealing of a twin-roll-cast Mg alloy. *Materials Characterization.* 114, 157-165. https://doi.org/10.1016/j.matchar.2016.02.019

[20] Montgomery, D. C. (2017). Design and analysis of experiments. *John Wiley & Sons.*